PROCEEDINGS OF SCIENCE

Experimental techniques for defect characterization of highly irradiated materials and structures

Ioana Pintilie[1*]
National Institute of Materials Physics
Str. Atomistilor 405A, Magurele, Ilfov
E-mail: ioana@infim.ro

Leona C. Nistor
National Institute of Materials Physics
Str. Atomistilor 405A, Magurele, Ilfov
E-mail: leonis@infim.ro

Sergiu V. Nistor
National Institute of Materials Physics
Str. Atomistilor 405A, Magurele, Ilfov
E-mail: snistor@infim.ro

Alexandra C. Joita
National Institute of Materials Physics
Str. Atomistilor 405A, Magurele, Ilfov
E-mail: alexandra.joita@infim.ro

There are several applications where solid devices are exposed to irradiation. Depending on the operational conditions (type of the particles, temperature, fluence) the physical properties of the exposed device degrades differently, reaching the point of electrical failure in very harsh enviroments. The radiation damage, starting already under low irradiation fluences, get more complex with increasing fluences due to the generation of various type of irradiation induced, electrically active, defects. Accordingly, the defect characterization becomes a more difficult and costly task, requiring several complementary techniques to understand the detailed relation between the "microscopic" reasons as based on defect analysis and their "macroscopic" consequences for device performance. In this respect, we present the most powerful techniques employed and developed within the CERN RD50 Collaboration for investigating highly irradiated materials/structures: (i) Thermally Stimulated Current and Thermally Dielectric Relaxation Current techniques used for electrical characterization of bulk and interface defect states. With the obtained defect parameters several electrical characteristics of the devices could quantitatively explained; (ii) High Resolution Transmission Electron Microscopy and Electron Paramagnetic Resonance allowing the structural and chemical identification of the radiation induced defects.

The 25th International workshop on vertex detectors
September 26-30, 2016
Location
La Biodola, Isola d'Elba, ITALY

[1]Speaker
[*] On behalf of the RD50 Collaboration.

© Copyright owned by the author(s) under the terms of the Creative Commons Attribution-NonCommercial-NoDerivatives 4.0 International License (CC BY-NC-ND 4.0).

PoS(Vertex 2016)033

1. Introduction

Segmented Silicon sensors are largely used in elementary particle and nuclear physics research at Large Hadron Collider (LHC) at the European Nuclear Research Centre CERN and in research with photons in free electron lasers [1,2]. However the impact of the large particle intensity leads to radiation damage effects in the material and hence to degradation in the detector performance, e.g. changes in the Charge Collection Efficiency (CCE), in the effective doping concentration (Neff) and hence depletion voltage, in the leakage current (LC) or carriers lifetimes [3-10] limiting their practical operation. While these effects can be barely tolerated in the present days LHC experiments, the applications in the planned LHC upgrade with a 10 times larger luminosity (HL-HLC) and consequently much larger radiation damage impose further challenges. The RD50 international collaboration at CERN "Development of Radiation Hard Semiconductor Devices for Very High Luminosity Colliders" is working for increasing the radiation tolerance of silicon detectors for their future use in HL-LHC experiments. The identification of the responsible radiation induced defects and understanding their generation and kinetics are of crucial importance for further developments of radiation hard silicon material. Projections for a long term guaranteed operation are only possible if the different damage parameters and their annealing dependence are intimately known. In this respect, it is worth noting that the electrical parameters of the defects are the input parameters in any attempt of simulating the device electrical characteristics [10-13]. Moreover, there are studies showing a strong dependence of these macroscopic damage effects on particle type and hence violating the Non Ionizing Energy Loss scaling hypothesis (NIEL) used so far to scale the damage produced by different particles with different energy [14-17]. Thus, the defect electrical characteristics, energy level in the bandgap of the irradiated material, its capture cross sections for electrons and holes, together with its concentration/generation rate after irradiation with different particles are the necessary defect parameters needed for calculating the impact on device characteristics [18]. Knowing also the defect chemical structure allows developing defect engineering strategies for diminishing the formation of detrimental defects or for generating other defects able to compensate the identified harmful effects. A good example of defect engineering is the enriching with oxygen of silicon, [19-23]. The most sensitive technique for electrical characterization of defects in semiconductors is the Capacitance Deep Level Transient Spectroscopy (C-DLTS). This method is however only applicable if a space charge region exists in the investigated device and the defect concentration is smaller than the doping of the semiconductor device. The method can be used on diodes and MOS like structures but not on resistor like bulk samples. Most of the presently known radiation induced defects, VO, V_2, C_i, C_iO_i, C_iC_s, IO_2, have been determined by C-DLTS [24] after low irradiation fluences ($\phi < 10^{12}$ cm^{-2}) where no changes in the devices electrically characteristics are usually observed at ambient temperatures. An exemption is the V_3 defect which generates LC [16, 25, 26]. However, using the electrical parameters of these defects and extrapolating their generation rates for larger fluences no correlation with the changes observed in the diodes electrical performance could be established. A straight conclusion was then that none of these defects are actually responsible for the devices degradation observed at fluences above 10^{12} cm^{-2} and most likely new types of radiation induced defects are created when increasing the fluence. Therefore, other methods, have to be employed to characterize the devices exposed to high irradiation levels. Suitable techniques employed within the RD50 collaboration are: Thermally

PoS(Vertex 2016)033

Stimulated Current (TSC) method, High Resolution Transmission Electron Spectroscopy (HR-TEM) and Electron Paramagnetic Resonance (EPR). These methods allow the detection and the electrical and structural characterization of the defects generated after high irradiation fluences.

2. Thermally Stimulated Current and Thermally Dielectric Relaxation techniques.

The TSC technique is allowing the detection and electrical characterization of radiation induced bulk defects in both, resistor like or diode like type of samples. Its sensitivity is limited by the presence of dark leakage current and the sensitivity of the current measurements instruments. In diode like structures, the TSC method is especially employed when the C-DLTS technique fails. The TSCexperimental procedure performed on a diode consists in the following steps: (i) the sample is cooled down to low temperature; (ii) at low temperature the filling of the traps with charge is performed by illumination or by forward biasing the diode; (iii) the sample, under a reverse bias, is heated up with a constant heating rate while measuring a discharging current due to the thermal emission of charge carriers from the traps. The obtained TSC spectrum consists in current peaks, each of them corresponding to a defect energy level in the forbiden bandgap of the investigated material. The filling of the traps can be also performed during cooling of the samples. However, the evaluation of TSC spectra measured on highly irradiated Si diodes deals with some severe problems which, if overlooked, can easily lead to erroneous results. Due to the large amount of different defects, the TSC spectra become very complex: the signals from different traps can strongly overlap, the diodes can not be fully depleted over the entire TSC temperature range, the change of the space charge sign (type inversion) can happen during the TSC measurement, the shape and the magnitude of the TSC peaks being altered substantially. The most critical aspect when measuring diodes is that the full depletion of the diode has to be guaranteed during the TSC measurement. Only this way the scanned volume of the sample is known and possible to be used for an accurate determination of the defects electrical parameters and concentration. Depending on the material doping and thickness, accurate results were provided by TSC for 1MeV neutrons equivalent fluences of up to ~ 10^{14} cm^{-2} for 300 μm thick STFZ (Standard Float Zone) silicon diodes and up to few times 10^{15} cm^{-2} for epitaxial silicon with thickness < 100 μm. Details about the requirements for a correct analysis of a TSC spectrum can be found in references [27-29]. Among several defects detected with this technique, widely employed within the RD50 Collaboration, there are some that prove to have a significant impact on the silicon diodes, being charged at ambient temperatures and thus, directly influencing N_{eff} [6, 7, 16, 21-23, 28]. Their electrical parameters, activation energy (Ea) and capture cross sections (σ) are given in Figure 1. The point defects are predominantly detected after high doses of gamma rays. In this case, the changes in both, LC and N_{eff} can be explained based on the electrical parameters and concentrations of only two defects, BD and I_p [21, 22]. The extended defects are strongly generated after hadron irradiation and they are fully responsible for the magnitude of N_{eff} and its annealing behavior [6, 7]. The changes in the LC however, are only partly explained after irradiation with high energy particles by the I_p and V_3 defects [6, 16, 25]. Therefore more experimental efforts have to be made in the future for detection and characterization of the defects generating currents in hadron irradiated devices.

The TDRC technique is a suitable method for determining the interface states (D_{it}) in MOS like structures. The experimental procedure is similar to TSC just that this time a

PoS(Vertex 2016)033

displacement current is measured, caused by the variation of the voltage dropping on the semiconductor/oxide interface and on the oxide, instead of a current related to the flow of free charge as in the TSC case. A very succesfull example of using the TDRC technique is given in Figure 2 along with the Capacitance/Conductance – Gate Voltage (C/G-V_g) characteristics measured on a Si/SiO_2 MOS capacitor exposed to 4.8 MGy of 12 keV X-rays at different annealing times at 80^0C. Using the procedure described in [30, 31] and the references there-in, from the TDRC spectra the energy distribution of interface states can be extracted and used to calculate the C/G-V_g characteristics.

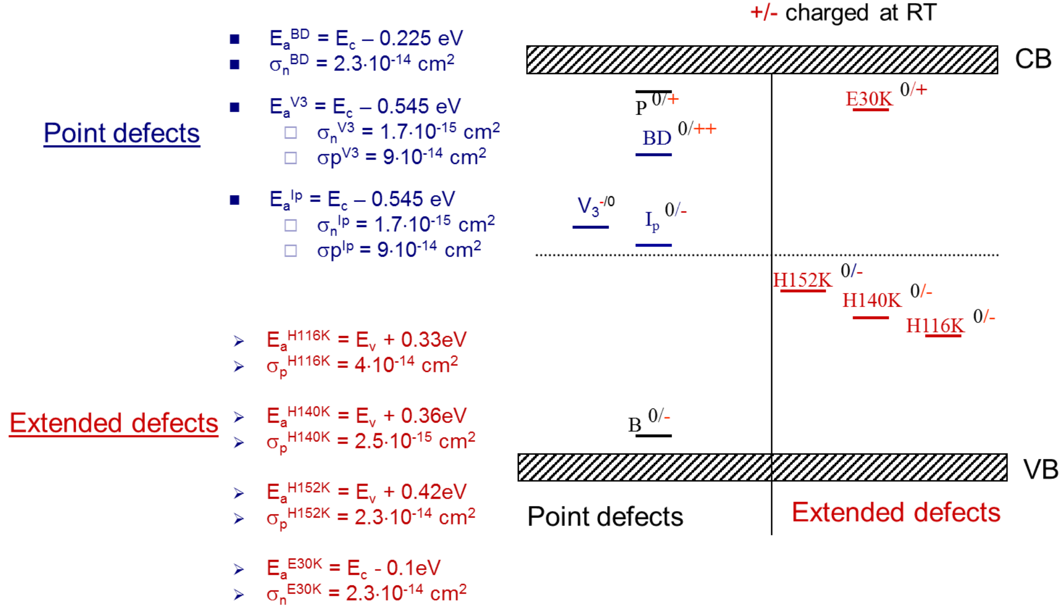

Figure 1. Radiation induced defects in silicon influencing N_{eff} and LC. P and B are the doping impurities used to fabricate the silicon p-n junctions. CB and VB stand for conduction and valence bands, respectively.

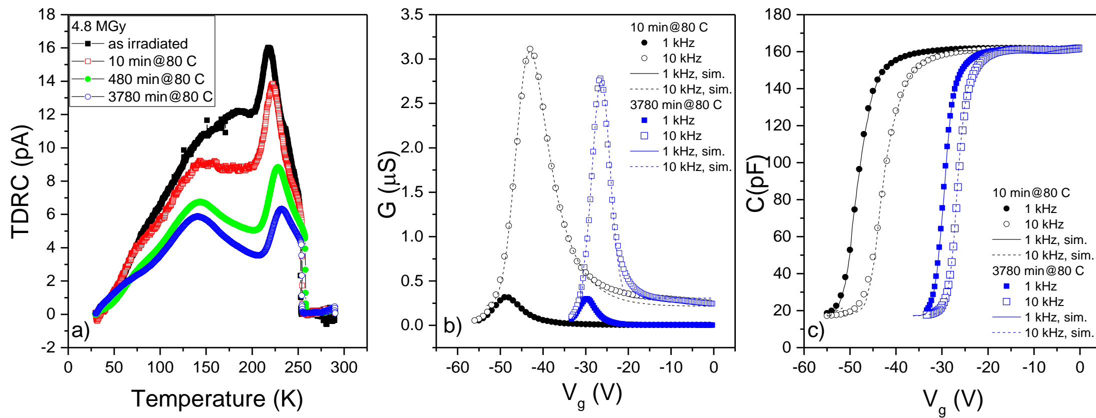

Figure 2. Si MOS capacitor exposed to 4.8 MGy of 12 keV X-rays: a) TDRC spectra measured after different annealing times at 80 ^{0}C; b) Conductance and c) Capacitance measured and calculated considering the three gaussian D_{it} energy distribution given in table I.

The TDRC spectra can be deconvoluted by considering minimum three gaussians, each of them corresponding to a certain energy distribution of D_{it}. The parameters of the three types of D_{it} considered are given in table I. As it can be observed, based on the TDRC measurements, both

PoS(Vertex 2016)033

the calculated C-V_g and G-V_g are very well fitting the experimental curves. Thus, similar to [30, 31], the simulations become accurate when the defect characteristics used as input parameters are experimentally determined.

Table I. Trapping parameters of the three dominant interface acceptor trapping levels considered to have a Gaussian energy distribution.

	D_{it}^1	D_{it}^2	D_{it}^3
capture cross section for electrons σ [cm^2]	(1.2 ± 0.8) ×10^{-15}	(5 ± 2.5) ×10^{-17}	(1.0 ± 0.05) ×10^{-15}
peak energy E_c-E_t [eV]	0.39 ± 0.005	0.48 ± 0.005	0.6 ± 0.01
FWHM [eV]	0.26 ± 0.005	0.13 ± 0.005	0.071 ± 0.001

3. High Resolution Transmission Electron Spectroscopy (HR-TEM)

Modern transmission electron microscopy (TEM) permits to study, down to atomic scale, the structure and chemical composition of almost any material with two conditions: to prepare a thin sample (100 – 10 nm) transparent to the electron beam and to prevent the electron beam damage of the sample during the observations. With the introduction of aberration-corrected lenses and of different spectroscopies based on the interaction of the electron beam with matter, the modern electron microscopes evolved to analytical instruments providing, with high spatial and spectral resolution, information of the position, nature and bond valance of the atoms in the material, incorporating a large range of techniques in a single instrument: high resolution TEM (HRTEM), electron diffraction, scanning TEM (STEM), electron filtered TEM (EFTEM), electron energy loss spectroscopy (EEELS) and energy dispersive X-ray spectroscopy (EDXS).

To illustrate the capabilities of advanced electron microscopy in the study of irradiation effects related to bulk radiation damage, we give here two examples, of irradiation with 27 MeV electrons and with 1 MeV neutrons of Standard Float-Zone (STFZ) silicon. In both cases, the specimens for TEM investigations were prepared in cross sections. The instrument used was a high resolution probe-corrected analytical JEOL JEM-ARM 200F operated at 200 kV with a resolution of 0.19 nm in HRTEM mode and of 0.08 nm in STEM mode. The microscope is equipped with a JEOL JED-2300T EDXS spectrometer and a Gatan GIF QuantumSE^{TM} Imaging Filter/EELS spectrometer. Previous studies, regarding the radiation damage produced by high energy electron irradiation of Si wafers, revealed the formation of clusters of point defects in the bulk of the silicon sample, most of them agglomerated either along the principal crystallographic directions or randomly, forming damaged regions with dimensions in the 2-5 nm range [16]. Here, we compare the damage effects produced by the irradiation with 27 MeV electrons and with 1 MeV neutrons. HRTEM images given in Figure 3 reveals the formation of a rather high density clusters of point defects, vacancies and interstitials in both of the samples. Only few are single/small clusters, meaning a single darker dot. Most of these single clusters of defects are agglomerated, either along the principal crystallographic directions, revealed by darker lines of clusters, or more randomly, seen as darker patches. The defect clusters are formed by accumulation of Si vacancies and self-interstitials, the end product of the collision cascade [16].

PoS(Vertex 2016)033

In the electron irradiated silicon sample single clusters of defects and small (2-3 nm) agglomerates of clusters of points defects along the <111> and <110> crystallographic directions forming star-like extended defects frequently appear. The insert in Figure 3a shows details of the star-like agglomerates of defects where the branches of the defect lie in the {111} planes. The contrast at an {111} defect results, according to Fedina [32], due to the accumulation of vacancies in this plane. The defect is further stabilized by a partial filling with interstitials. On the other hand, in the neutron irradiated sample (Figure 3b) prevail the more randomly agglomerated clusters of point defects, forming larger disordered regions of ~4 nm (dark patches) marked by red arrows. A HRTEM image at higher magnification of such a complex extended defect (dark patch) is given in the inset. The defect, marked by red arrow, lies in three successive {110} planes where the Si lattice is very disturbed. This defect might be a precursor of the {113} defect formed by agglomeration of self-interstitials, observed in FZ silicon by prolonged irradiation with 2 MeV electrons [33] which, in the first stage accumulate along the <110> direction and then nucleate in the {113} planes [34]. Worth to notice that in both silicon samples irradiated with energetic particles, the observed structure of the damaged zones is highly disturbed, but not completely amorphous.

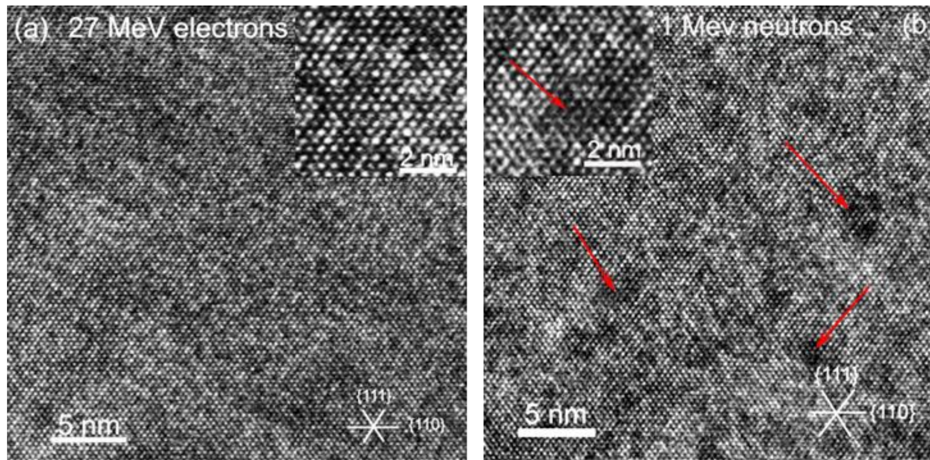

Figure 3. HRTEM images along the [110] zone axis revealing the radiation damage produced in STFZ Si by: a) 27 MeV electrons (ϕ=2x10^{16} cm^{-2}); b) 1 MeV neutrons (ϕ=1x10^{16} cm^{-2}).

4. Electron Paramagnetic Resonance (EPR) technique

The EPR technique is one of the most powerful tools for evidencing the presence and determining the atomic structure of the paramagnetic point defects produced by irradiation in semiconductors [35, 36]. Since the first reported use of EPR to characterize the radiation induced paramagnetic point defects (IPPDs) in Si [37] more than 400 paramagnetic point defects have been reported so-far [38-40]. Their spectra parameters, local symmetry and proposed structural models are tabulated in the Landolt-Boernstein Database [37] and in the Defect Dat@base from the University of Tsukuba, Japan [40]. In the EPR experiments one investigates the transitions induced by an electromagnetic field with frequency in the microwave region (usually 9 – 34 GHz) between the Zeeman levels associated with the magnetic moment of the unpaired electrons with total spin $S \neq 0$ of the investigated IPPD. The orbital moment of the electron, as well as its associated spin-orbit interaction, determines the coupling of the crystal field with the electron

PoS(Vertex 2016)033

spin, explaining the high sensitivity of the EPR spectra to the orientation of the Zeeman magnetic field with respect to the crystal axes (or to the local symmetry axes of the defect). As a result, the EPR spectra are usually strongly anisotropic, the angular dependence of the transition fields (or the line positions in the usual Zeeman field scan procedure for recording the EPR spectra) obtained at rotations of the magnetic field in a crystal plane reflect the defect local symmetry and therefore offer essential information about the atomic structure of the investigated defect. The EPR spectra line positions of the IPPDs in Si are usually described by the spin Hamiltonian (SH) with usual notations [35]:

$$H_{SH} = \mu_B\, S \cdot g \cdot B + S \cdot D \cdot S + \Sigma_j\, (S \cdot A_j \cdot I_j) \qquad (1)$$

The first term in (1) describes the interaction between the electron spin **S** and the external magnetic (Zeeman) field B, its magnitude and symmetry being determined by the *g*-tensor. The second term, which is included only for S> ½, takes into consideration the local crystal field influence on the electron wave function, its magnitude being determined by the *D*-tensor. The third term describes the hyperfine (*hf*) interaction between the electron spin S and the magnetic moment associated with the nuclear spin I_j of the j-th atom involved in the IPPD structure. Irradiation with light, of various energies, in particular larger than the Si band gap, may change the charge state of a defect, uncovering the presence of normally EPR silent defects, offering information about the level structure in the gap and the properties of other charge states [41].

The presently reported EPR investigations have been performed in the microwave frequency Q (34 GHz) - band, from room temperature (RT) down to 10 K, with the ELEXSYS-E500Q (Bruker) spectrometer equipped with a high sensitivity probe head and a cryostat operating from 3.6 K up to RT, with nominal sensitivity of $1.2x10^9$ spins/Gauss. Details about the equipment and magnetic field calibration procedures are given in [42]. The EPR measurements were performed on STFZ samples of 4 x 1.8 x 0.3 mm^3 size with the longest side parallel to one of the <110> crystal axes, allowing rotations of the magnetic field in the perpendicular (110) plane. The samples were cut from Si wafer with impurity concentration values: [O] = 10^{16} cm^{-3}; [C] = $2x10^{15}$ cm^{-3}, [P] = 10^{12} cm^{-3}, irradiated at RT with 27 MeV (ϕ= $2x10^{16}$ cm^2) and 3.5 MeV electrons (ϕ=10^{17} cm^2). We found out that a large number of anisotropic EPR lines could be observed only during band to band illumination of the samples at lower temperatures (T < 150 K). Consequently we developed an *in-situ* illumination set-up using as a coherent light source a thermally stabilized pig tailed laser diode model LPS-1060-FC from Thorlabs, with 60 mW maximum output power. The resulting light was sent with minimum loss (< 3 %) to the sample through a optical fiber inserted in the sample rod coupled to the goniometer head.

The EPR measurements on the as-irradiated samples, performed from RT down to 10K, did reveal the presence of only a few low intensity isotropic signals, similar to those previously observed in STFZ irradiated with 6MeV electrons [43]. The in-situ illumination in the 90 K < T < 150 K temperature range resulted in the observation of new, anisotropic lines. Examples for 3.5 MeV and 27 MeV electron irradiated samples are given in Figure 4. Based on the quantitative analysis we could determine the local symmetry and SH parameters of the paramagnetic centers responsible for the observed spectra (Table II). Comparing our results with published data [39, 40] one could identify the accepted structural model of the corresponding IPPDs. Table II presents, besides the name/structure, the SH parameters and local symmetry of the identified IPPDs, as well as the measuring temperature and irradiation conditions (type, energy). Examining the spectra from Figure 4 one finds differences between the production rate of the IPPDs in the

PoS(Vertex 2016)033

STFZ irradiated with 3.5 and 27 MeV electrons. Thus, the G7 / $[V_2]^-$ and PK1 $[V_5]^-$ centers are present in both samples, although the concentration of the PK1 centers is much smaller in the 27 MeV irradiated sample. There are also IPPDs, namely A16 and B5 / $[I_3]$, which can be observed only in the 3.5 MeV irradiated samples. Meanwhile the A3 /P3 $[V_4]^-$ defect is present only in the EPR spectra of the 27 MeV irradiated samples. The G7 negatively charged divacancy, which exhibits at low temperatures (T < 80K) a monoclinic symmetry, is subjected at higher temperatures to a thermally activated reorientation from one Jahn-Teller distortion direction to another, resulting at T > 110K in a motional averaged spectrum with axial symmetry [38]. The two states are observed in our EPR spectra recorded at T=50 K and 120 K, respectively. The presence of these centers has been reported in both electron and neutron irradiated STFZ [39]. The A16 center with orthorhombic symmetry has been reported for the first time in electron irradiated Cz-Si [41]. Because of the close g-values and the same symmetry as for the A15 / $[V_3\text{-}O_3]^0$ center it has been suggested to have a related structure. It is interesting to note that we are observing the A16 center in oxygen lean STFZ, where the presence of other V-O related centers, such as B1/A (V-O) or A14 / $[V_2\text{–}O]^-$ is not observed. One could therefore speculate that A16 is rather related to the A4 / $[V_3]^-$ center, which also exhibits orthorhombic symmetry and close g – values. One should mention that the fitting g-values (2.0067; 2.0035; 2.0108) for the angular dependence of our so called A16 spectrum are somehow different from those reported for the A16 center: 2.0071; 2.0036; 2.0112 [44], but also different from those of the A4/$[V_3]^-$ center: 2.0059; 2.0030; 2.0094 [45].

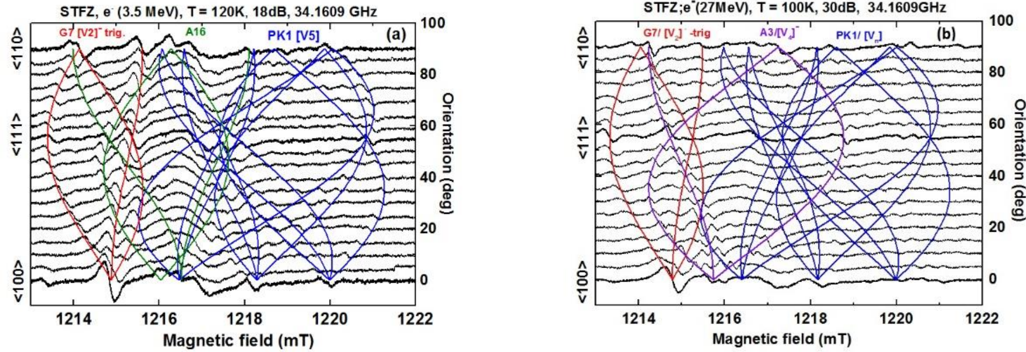

Figure 4. EPR spectra on STFZ samples irradiated with 3.5 MeV and 27 MeV electrons.

Table II. The principal characteristics of the IPPDs evidenced by EPR in the STFZ samples irradiated with electrons of 3.5 and 27 MeV.

IPPD	**g - values**	**Symmetry**	**T_{meas}**	**Irrad. conditions**
G7 / $[V2]^-$	2.0012; 2.0135; 2.0150	Trigonal	100-120 K	e^- (3.5 and 27 MeV)
G7 / $[V2]^-$	2.0080; 2.0080; 2.0117	Monoclinic-I	< 50 K	e^- (3.5 and 27 MeV)
A16	2.0067; 2.0035; 2.0108	Orthorh.-I	90 -120 K	e^- (3.5 MeV)
PK1/ $[V5]^-$	2.0085; 2.0042; 1.9986	Triclinic	50-120 K	e^- (3.5 and 27 MeV)
A3 / $[V4]^-$	2.0102; 2.0102; 2.0028	Trigonal	100 K	e^- (27 MeV)
B5/ [I3]	2.0079; 2.0079; 2.0014	Trigonal	50 K	e^- (3.5 MeV)

PoS(Vertex 2016)033

The EPR investigations at $T < 120$ K, with in-situ across the band illumination using intense 1.06 micron laser light, revealed the presence in the STFZ samples irradiated with 3.5 MeV and 27 MeV electrons of several IPPDs, some of them not previously reported under the present combination of Si samples and type of irradiation. As expected for true oxygen lean materials, with one exception, the observed IPPDs in our investigated STFZ are vacancies in various states of aggregation as di-, quadri- and penta-vacancies. We could also observe, for the first time in electron irradiated Si the formation of the tri-interstitial B5/[I_3] defect. Finally, one should mention that the formation of the A16 defect in such circumstances raises serious doubts about its suggested structure containing oxygen atoms.

5. Summary and Outlook

The experimental techniques employed within the RD50 collaboration for defect characterization after high radiation levels of silicon based devices were briefly described along with a few examples of their applications. Unfortunatelly, there is no method to use for determining all we need to know about the radiation induced defects and the connection between the results given by different techniques is not straightforward. The radiation damage gets more very complex with increased fluence values, the defect characterization is more difficult and time consuming, requiring several complementary techniques to understand and predict the changes in the device performance. The TSC and TDRC techniques are suitable for characterizing defects from electrical point of view. When the electrically active defects can be detected and fully characterized by determining their energy levels in the bandgap of the irradiated material, their capture cross-sections for electrons and holes as well as the dependence of their concentration on fluence and type of the particles, then it is possible to perform reliable simulations for predicting the device behaviour in different operational scenarious. These methods can detect electronic size defects (like the interface states are), point defects (atomic size) or extended defects (clusters of atomic defects). The HRTEM is a powerfull technique for tracking the structural changes caused by the generation of clusters of defects and their annealing. The EPR method gives information about the structural and chemical composition of point defects generated in very large concentrations, above 10^{16} cm^{-3}. However, there are several difficulties in getting all the information one would like and further correlated studies should be performed.

Acknowledgements

The authors gratefully acknowledge the financial support from the Romanian Authority for Scientific Research through the Project PCE72/5.10.2011.

References

[1] F. Gianotti, M. L. Mangano, and T. Virdee, *Physics potential and experimental challenges of the LHC luminosity upgrade,* Eur. Phys. J. C **39** (2005), 293.

[2] H. N. Chapman, et al., *Femtosecond time-delay X-ray holography*, Nature, **448** (2007), 676.

[3] E. Fretwurst, et al., *Recent advancements in the development of radiation hard semiconductor detectors for S-LHC*, Nucl. Instr. & Meth. Phys. Res. A **552** (2005), 7.

PoS(Vertex 2016)033

[4] G. Kramberger, et al., *Comparison of pad detectors produced on different silicon materials after irradiation with neutrons, protons and pions*, Nucl. Instr. & Meth. Phys. Res. A **612** (2010), 288.

[5] A. Affolder, et al., *Charge collection efficiencies of planar silicon detectors after reactor neutron and proton doses up to 1.6 x 10^{16} n(eq) cm^{-2}*, Nucl. Instr. & Meth. Phys. Res. A **612** (2010), 470.

[6] I. Pintilie, G. Lindstroem, A. Junkes and E. Fretwurst, *Radiation Induced Point and Cluster-Related Defects with Strong Impact to Damage Properties of Silicon Detectors*, Nucl. Instr. & Meth. Phys. Res. A **611** (2009), 52.

[7] I. Pintilie, E. Fretwurst and G. Lindström, *Cluster related hole traps with enhanced-field-emission – the source for long term annealing in hadron irradiated Si diodes*, Appl. Phys. Lett. **92** (2008) 024101

[8] **V**. Rumbauskas, D. Meskauskaite, T. Ceponis and E. Gaubas, *Anneal induced transforms of radiation defects in heavily electron irradiated Si diodes*, J. Instrum. **11** (2016) P09004

[9] A. Tekorius, E. Gaubas, T. Ceponis, J. Pavlov, J. Vaitkus, M. Glaser, and M. Moll, *Fluence and anneal dependent variations of recombination parameters in Si irradiated by 26 GeV protons*, Conf. Proc. *"*Radiation Interaction with Materials: Fundamentals and Applications 2014*"* (2014), 432-435.

[10] V. Eremin, E. Verbitskaya, and Z. Li, *The origin of double peak electric field distribution in heavily irradiated silicon detectors*, Nucl. Instr. & Meth. Phys. Res. A **476** (2002)**,** 556–564.

[11] R. Dalal, A. Bhardwaj, K. Ranjan, K. Lalwani and G. Jain, *Simulation of Irradiated Si Detectors*, PoS(Vertex2014) 030.

[12] F. Moscatelli, D. Passeri, A. Morozzi, R. Mendicino, G.-F. Dalla Betta, and G. M. Bilei, *Combined Bulk and Surface Radiation Damage Effects at Very High Fluences in Silicon Detectors: Measurements and TCAD Simulatio*ns, IEEE Trans. Nucl. Sci., **63**, (2016), 2716–2723.

[13] J. Schwandt, *Validation strategy for the simulation of highly irradiated silicon pixel sensors,* 29th RD50 Workshop, 21-23 of November, 2016.

[14] M. Huhtinen, *Simulation of non-ionising energy loss and defect formation in silicon*, Nucl. Instr. & Meth. Phys. Res. A **491** (2002), 194.

[15] C. Inguimbert and P. Arnolda, T. Nuns and G. Rolland, *Effective niel in silicon: Calculation usingmolecular dynamic results*, IEEE Trans. NS **57** (2010), 1915.

[16] R. Radu, I. Pintilie, L. C. Nistor, E. Fretwurst, G. Lindström and L. F. Makarenko, *Investigation of point and extended defects in electron irradiated silicon - Dependence on the particle energy*, J. Appl. Phys. **117** (2015) 164503.

[17] A. Ruzin, G. Casse, M. Glaser, A. Zanet, F. Lemeilleur and S.Watts, *Comparison of radiation damage in silicon induced by proton and neutron irradiation*, IEEE Trans. Nucl. Sci. NS **46** (1999), 1310.

[18] T. Peltola, *Silicon sensors for trackers at high-luminosity environment,* Nucl. Instr. & Meth. Phys. Res. A **796** (2015), 74.

[19] Z. Li, B. Dezillie, M. Bruzzi, W. Chen, V. Eremin, E.Verbitskaya and P. Weilhammer, et al., *HTLT oxygenated silicon detectors: radiation hardness and long-term stability*, Nucl. Instr.& Meth. Phys. Res. A **461** (2001), 126.

[20] G. Lindstroem, *Developments for radiation hard silicon detectors by defect engineering-results by the CERN RD48 (ROSE) collaboration*,Nucl. Instr. & Meth. Phys. Res. A 465, 60 (2001).

[21] I. Pintilie et al, *Second-order generation of point defects in gamma-irradiated float-zone silicon, an explanation for "type inversion",* Appl. Phys. Lett. 82 (2003) 2169.

[22] I. Pintilie, E. Fretwurst, G. Lindström and J. Stahl, *Results on defects induced by 60Co gamma irradiation in standard and oxygen-enriched silicon*, Nucl.Instr. & Meth. Phys.Res. A **514** (2003), 18.

PoS(Vertex 2016)033

[23] I. Pintilie, E. Fretwurst, G. Lindström and J. Stahl, *Close to midgap trapping level in 60Co gamma irradiated silicon detectors*, Appl. Phys. Lett. **81** (2002) 165.

[24] A. Hallen, N. Keskitalo, F. Masszi, and V. Nagl, *Lifetime in proton irradiated silicon*, J. Appl. Phys. **79** (1996), 3906.

[25] A. Junkes, D. Eckstein, I. Pintilie, L. F. Makarenko and E. Fretwurst, *Annealing study of a bistable cluster defect*, Nucl. Instr. & Meth. Phys. Res. A **612** (2010) 525 - 529.

[26] V. P. Markevich et al., *Trivacancy and trivacancy-oxygen complexes in silicon: Experiments and abinitio modeling*, Phys. Rev. B **80** (2009) 235207.

[27] I. Pintilie, L. Pintilie, M. Moll, C. Tivarus, E. Fretwurst and G. Lindstroem, *Thermally stimulated current method applied on diodes with high concentration of deep trapping levels*, Appl. Phys. Lett. **78** (2001), 550.

[28] I. Pintilie, M. Buda, E. Fretwurst, G. Lindstroem and J. Stahl, *Stable radiation-induced donor generation and its influence on the radiation tolerance of silicon diodes*, Nucl. Instr. & Meth. Phys. Res. A **556** (2006), 197.

[29] I. Pintilie, C. Tivarus, T. Botila, D. Petre and L. Pintilie, *Experimental evidence of deep electron and hole trapping levels in high fluence proton irradiated p-n Si junctions using Optical Charging Spectroscopy*, Nucl. Instr. & Meth. Phys. Res. A **439** (2000), 221.

[30] I. Pintilie, C. M. Teodorescu, F. Moscatelli, R. Nipoti, A. Poggi, S. Solmi, L. S. Løvlie and B. G. Svensson, *Analysis of electron traps at the 4H–SiC/SiO2 interface; influence by nitrogen implantation prior to wet oxidation*, J. Appl. Phys. **108** (2010), 024503.

[31] J. Zhang, I. Pintilie, E. Fretwurst, R. Klanner, H. Perrey and J. Schwandt, *Study of radiation damage induced by 12 keV X-rays in MOS structures built on high-resistivity n-type silicon*, J. Synchrotron Rad. **19** (2012), 340.

[32] L Fedina, A. Gutakovskii, A. Aseev, J. Van Landuyt and J Vanhellemont, *On the mechanism of {111}-defect formation in silicon studied by in situ electron irradiation in a high resolution electron microscope*, Phil. Mag. A **77** (1998), 423.

[33] S. Takeda, *Structure Analysis of Defects in Nanometer Space Inside a Crystal: Creation and Agglomeration of Point Defects in Si and Ge Revealed by High-Resolution Electron Microscopy*, Micr. Res. & Techn. **40** (1998), 313.

[34] S. Takeda and T. Kamino, *Agglomeration of self-interstitials in Si observed at 450 ^{o}C by high-resolution transmission electron microscopy*, Phys. Rev. B **51**, (1995-II), 2148-2152.

[35] J. M. Spaeth and H. Overhof, *Point Defects in Semiconductors and Insulators*, Springer Series in Materials Science, vol. **51**, eds. R. Hull, R. M. Osgood and J. Parisi, Springer, 2003.

[36] S. V. Nistor, M. Stefan, D. Ghica and E. Goovaerts, *Multifrequency ESR characterization of paramagnetic point defects in semiconducting cubic BN crystals*, Appl. Magn. Res. **39** (2010), 87-101

[37] A. M.Portis, A. F. Kip, C. Kittel and W. H. Brattain, *Electron Spin Resonance in a Silicon Semiconductors*, Phys. Rev. **90** (1953), 988.

[38] G.D.Watkins, *EPR of defects in semiconductors;Past, present, future*. Phys.Sol. State **41** (1999) 746

[39] Landolt-Bornstein – Group III Semiconductors –vol. 41, subvolume A2a, Group IV Elements-Impurities and Defects, in Group IV Elements, IV-IV and III-V Compounds. Silicon Paramagnetic Centers, Springer Materials Series, Springer, Berlin

[40] T. Umeda, S. Hagiwara, M. Katagiri, N. Mizuochi and J. Isoya, *A web-based database for EPR centers in semiconductors*. Physica B 376-377, 249-252 (2006);

PoS(Vertex 2016)033

[41] J. W. Corbett, *Electron Radiation Damage in Semiconductors and Metals*, in Solid State Physics, vol. **7**, Eds. F. Seitz and D. Turnbull, Acad. Press New York and London, 1966.

[42] S. V. Nistor and M. Stefan, *In-depth investigation of Mn2+ ions EPR spectra in ZnS single crystals with pure cubic structure*, J. Phys.: Condens. Matter 21 (2009), 145408.

[43] S. V. Nistor, D. Ghica, I. Pintilie and E. Manaila, *Paramagnetic point defects in pure and ^{13}C and ^{17}O implanted silicon for high energy particle detectors*, Rom. Repts. Phys. **65** (2013), 825.

[44] Y. H. Lee and J. W. Corbett, *EPR studies of defects in electron-irradiated silicon: Atriplet state of vacancy-oxygen complexes*, Phys. Rev. B **13** (1976), 2653-2666

[45] Y. H. Lee, Y. M. Kim and J. W. Corbett, *New EPR spectra in neutron-irradiated silicon*, Rad. Effects 15 (1972), 77.

PoS(Vertex 2016)033